Geophys. J. Int. (2006) **167,** 1005–1016 doi: 10.1111/j.1365-246X.2006.03126.x

Stable and unstable damage evolution in rocks with implications to fracturing of granite

Yariv Hamiel,[1,2] Oded Katz,[2] Vladimir Lyakhovsky,[2] Ze'ev Reches[3] and Yuri Fialko[1]

[1] *Institute of Geophysics and Planetary Physics, Scripps Institution of Oceanography, University of California, San Diego, La Jolla,* CA 92093, *USA. E-mail: yarivh@ucsd.edu*

[2] *Geological Survey of Israel, Jerusalem* 95501, *Israel*

[3] *School of Geology and Geophysics, University of Oklahoma, Oklahoma* 73019, *USA*

Accepted 2006 July 3. Received 2006 June 21; in original form 2006 February 27

SUMMARY

We address the relation between the rock rigidity and crack density by comparing predictions of a viscoelastic damage rheology model to laboratory data that include direct microscopic mapping of cracks. The damage rheology provides a generalization of Hookean elasticity to a non-linear continuum mechanics framework incorporating degradation and recovery of the effective elastic properties, transition from stable to unstable fracturing, and gradual accumulation of irreversible deformation. This approach is based on the assumption that the density of microcracks is uniform over a length scale much larger than the length of a typical crack, yet much smaller than the size of the entire deforming domain. For a system with a sufficiently large number of cracks, one can define a representative volume in which the crack density is uniform and introduce an intensive damage variable for this volume. We tested our viscoelastic damage rheology against sets of laboratory experiments done on Mount Scott granite. Based on fitting the entire stress–strain records the damage variable is constrained, and found to be a linear function of the crack density. An advantage of these sets experiments is that they were preformed with different loading paths and explicitly demonstrated the existence of stable and unstable fracturing regimes. We demonstrate that the viscoelastic damage rheology provides an adequate quantitative description of the brittle rock deformation and simulates both the stable and unstable damage evolution under various loading conditions. Comparison between the presented data analysis of experiments with Mount Scott granite and previous results with Westerly granite and Berea sandstone indicates that granular or porous rocks have lower seismic coupling. This implies that the portion of elastic strain released during a seismic cycle as brittle deformation depends on the lithology of the region. Hence, upper crustal regions with thick sedimentary cover, or fault zones with high degree of damage are expected to undergo a more significant inelastic deformation in the interseismic period compared to 'intact' crystalline rocks.

Key words: cracked media, damage, fractures, rheology.

INTRODUCTION

Laboratory investigations of rock fracturing indicate that damage starts to develop well before the rock fails. The evolution of damage profoundly affects the mechanical properties of rocks (e.g. Nishihara 1957; Zoback & Byerlee 1975; Schock 1977; Lockner & Byerlee 1980; Reches & Lockner 1994; Pestman & Munster 1996; Rubinstein & Beroza 2004), and decreases their elastic moduli at relatively large stresses prior to failure (e.g. Lockner & Byerlee 1980; Lockner *et al.* 1991, 1992; Fialko *et al.* 2002; Fialko 2004; Katz & Reches 2004). In order to simulate the observed degradation of the effective elastic properties, a non-dimensional scalar or tensor damage variable is introduced in continuum damage rheology models. The damage variable characterizes a properly chosen volume of rock so that the density of internal flaws (e.g. microcracks in a laboratory specimen or small faults in the Earth's crust) within this volume may be considered uniform. This paper focuses on the application of damage rheology to the failure of brittle granite. According to damage mechanics, the change in the intensity of the damage variable is proportional to the change in the rigidity of the rock. However, the relation between rock rigidity and microcrack density has not been clear, and our main objective here is to construct these relations.

Microcrack density in brittle rocks was evaluated by acoustic emission analysis (e.g. Lockner *et al.* 1991; Zang *et al.* 1996; Janssen *et al.* 2001), and by direct microstructural analyses of microfractures

and dilatational microcracks (Hadley 1976; Tapponnier & Brace 1976; Kranz 1979; Moore & Lockner 1995; Homand *et al.* 2000; Oda *et al.* 2002; Katz & Reches 2004). Only a few attempts have been made to compare experimentally obtained microcrack density with theoretical damage parameters. Katz & Reches (2004) presented experimental evidence for the relations between experimentally measured microcracks density and the reduction of the elastic moduli of granite rock samples. Hamiel *et al.* (2004a) constrained the viscoelastic parameters of damage rheology by using triaxial laboratory experiments done on samples of Westerly granite and Berea sandstone. They found clear correlation between simulated damage and accumulated acoustic emission recorded during the loading of the samples. Based on these results we hypothesize that the microcrack density is directly proportional to the damage variable in the damage rheology presented by Lyakhovsky *et al.* (1997a) and Hamiel *et al.* (2004a). The present study quantitatively compares the predictions of the damage rheology with laboratory data that include stress–strain relations and direct microscopic mapping of microcracks.

BACKGROUND

The theory of damage mechanics has been extensively applied to model the deformation of brittle solids as well as large-scale geodynamic processes (e.g. Rabotnov 1988; Ben-Avraham & Lyakhovsky 1992; Kachanov 1994; Lyakhovsky *et al.* 1994; Ben-Avraham *et al.* 1995; Krajcinovic 1996; Skrzypek & Ganczarski 1999). Weinberger *et al.* (2000) demonstrated a good agreement between field-observed deformation around *en-echelon* dike segments in porous sandstone and damage-based simulations. Ben-Zion *et al.* (1999), Lyakhovsky *et al.* (2001) and Ben-Zion & Lyakhovsky (2002) used damage rheology to understand the deformation associated with earthquake cycles, evolving fault geometries, frequency-size statistics of earthquakes, and accelerated seismic release (see also review by Rundle *et al.* 2003). Shcherbakov & Turcotte (2004) and Ben-Zion & Lyakhovsky (2006) applied damage mechanics to explain the decay of aftershock sequences. Damage mechanics also used to study irreversible deformation in a brittle layer on the top of a convecting mantle (Bercovici 2003; Regenauer-Lieb & Yuen 2003; Auth *et al.* 2003; Bercovici & Ricard 2005; Nanjo *et al.* 2005).

Several researchers (see review by Kachanov 1994) proposed damage models with a scalar damage variable that fit various aspects of existing experimental results. In the study of Hansen & Schreyer (1994), a scalar isotropic damage model correlated well with changes of Young's modulus but not with changes of the apparent Poisson ratio. For this reason, Ju (1990) and Hansen & Schreyer (1994) suggested upgrading the damage variable from a scalar to a tensor quantity. Such a tensorial damage model contains at least three adjustable parameters that can be used to simulate the evolution of the apparent Poisson ratio. Variations of Young's modulus and Poisson's ratio with damage intensity under different types of load can also be described using a non-linear elastic model with scalar damage variable. This was done in the damage model proposed by Lyakhovsky & Myasnikov (1985). Lyakhovsky & Myasnikov (1985) established a thermodynamical foundation for a rheological model of damaged material by using the balance equations of energy and entropy (see also Myasnikov *et al.* 1990; Lyakhovsky *et al.* 1993, 1997a). They developed a scalar damage model that accounts for non-linear elasticity by adding an additional second-order term to the free energy of elastic solid, and connected the evolving elastic moduli to a single damage variable. Hamiel *et al.* (2004a) generalized the framework to a viscoelastic damage model with power-law relation between the damage variable and the effective elastic properties. Hamiel *et al.* (2004b, 2005a) incorporated the damage rheology with Biot's poroelasticity, and described the coupled evolution of damage and porosity in high porosity rocks. A thermodynamically approach was also used as the basis of other damage models (e.g. Valanis 1990; Papa 1993; Hansen & Schreyer 1994; Kachanov 1994; Krajcinovic 1996). Fibre-bundle models of damage (Newman & Phoenix 2001; Shcherbakov & Turcotte 2003; Turcotte *et al.* 2003) have similar ideas with torn fibres corresponding to cracks. Frictional frameworks have an analogous physical concept expressed in terms of the contact area. This allowed Lyakhovsky *et al.* (2005) to develop quantitative relations between observed phenomenology of the rate- and state-dependent friction and the damage rheology of Lyakhovsky *et al.* (1997a) and Hamiel *et al.* (2004a).

EXPERIMENTAL SETTING AND RESULTS

The experiments and microstructural analysis of Katz *et al.* (2001) and Katz & Reches (2004) provide an outstanding database to verify and constrain the damage model. These authors used 25.4-mm-diameter cylinders of the medium-grained (0.9 ± 0.2 mm) Mount Scott Granite to perform two series of triaxial tests. In the first series, the samples were loaded to failure from uniaxial to 66 MPa confining pressures (Katz *et al.* 2001). In the second series of experiments, the samples were held at a constant stress after loading, a procedure termed load-hold tests (Katz & Reches 2004). In these tests, the confining pressure was 41 MPa, for which the ultimate strength, $U_S = (\sigma_1 - \sigma_2)$, is 586 ± 16 MPa. Each load-hold test consists of four steps:

(i) Confining pressure loading at a constant rate of 0.023 MPa s^{-1}.

(ii) Axial loading to the pre-selected stress that ranges from $0.54 \cdot U_S$ to $1.05 \cdot U_S$. Axial shortening was at a strain rate of $\sim 10^{-5}$ s^{-1}.

(iii) Once the pre-selected stress was achieved, the specimen was held at a constant stroke for up to 6 hr.

(iv) After the hold period, the samples were unloaded by first reducing the axial stress to the confining pressure and then decreasing both stresses at the loading rates.

During the experiments, load, axial and transversal strains were continuously monitored. One of the advantages of these sets of experiments is the different loading path. The experimental loading path for the different tests is schematically shown in Fig. 1. After unloading four selected samples were analysed for microstructural damage induced by loading (Fig. 2 and Table 1). One non-loaded sample (sample 123) was also analysed in order to obtain the initial microcrack density of the initial rock. Together with the non-loaded sample the all five analysed samples were selected in a way that they will span the whole loading path, from the initial damage in the non-loaded sample (sample 157) via onset of damage accumulation (sample 123) to total failure (sample 110). This microstructural mapping was conducted by simultaneous examination of the fracture on a petrographic microscope and mapping on the digitized image of the scanned thin section. The cylindrical samples and thin-section preparation was done in a very careful manner in order to avoid damage in preparation stage including coring with minimal normal loading (i.e. very slow advancing of the drill-bid), thin-section preparation after the cylindrical-samples were cast and confined in epoxy, and cutting of the samples with minimal load

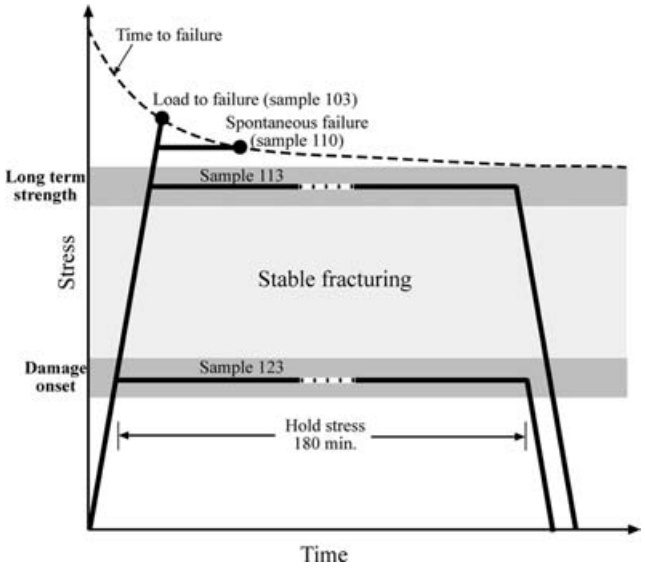

Figure 1. Schematic diagram of the loading and types of experiments. Dark grey areas represent some variability in the onset of damage and the long term strength as deducted from the experiments. Light grey area represents the region where the damage evolution has steady-state solution, and dashed line represents the time-to-failure curve. The sample numbers denote experiments performed at different conditions.

of the cutting-disk (for more details see Katz & Reches 2004). The mapping provided the mode, dimensions, density and distribution of stress-induced microfractures (Katz & Reches 2004). The digitized microstructural data was also used to generate fracture maps and to calculate a dimensionless microcrack density. Following Kachanov (1992), the microcrack density, ρ_c, is defined as a sum of squared length of all the mapped microcracks normalized to the representative area:

$$\rho_c = \frac{l}{A}\sum_n L_n^2, \tag{1}$$

where A is the representative area, L_n is a half-length of the crack number n. Spatial distribution of the microcracks density, ρ_c, calculated for five analysed samples using eq. (1) and the microfracture maps of Katz & Reches (2004) are shown in Fig. 2. The average microcracks density and standard deviation for each sample given in Table 1 is calculated over 20–30 sub-regions covering each microfracture map. The microcracks density value given for each sample is an average of four values representing each quarter of the mapped thin section. The local value of ρ_c for the non-loaded sample 157 (Fig. 2a) and sample 123 (Fig. 2b) varies gradually from 0 to 0.15 without clear localization. Microcrack distribution significantly localizes in samples loaded to higher stress, that is, sample 114 (Fig. 2c) that was loaded up to 0.88 of the rock strength and samples 113 and 110 (Fig. 2d, e) that was loaded up to 0.95 of rock strength. This observation, in agreement with laboratory results reported by Lockner *et al.* (1992), indicates that microcracks tend to localize only at relatively high stress, close to failure. Based on their maps Katz & Reches (2004) concluded that the rock sample fails when the patches of localized damage grow and consolidate into a continuous damage zone cutting the strong matrix. The shape of the damage zone of the failed sample 110 (Fig. 2e) confirms that the fault zone was initiated in the area of highest microcracks density and propagated out of this zone toward the edges of the sample.

The different types of experiments allow investigating rock deformation under different types of loading and regimes of fracturing. All samples loaded below 95 per cent of the rock strength remained stable during the entire hold stage in spite of increase of the microcrack density and material degradation. Most of the samples loaded to higher stresses failed, but not instantaneously. For example, it took as long as 61 minutes for sample 104 (see Table 1 in Katz & Reches 2004) to fail spontaneously under constant hold stress of 613 MPa. These results explicitly demonstrate a transition from stable to unstable fracturing previously discussed by Kranz *et al.* (1982), Lawn (1993), Martin & Chandler (1994) and others in context of static fatigue tests. Additional mechanical data on the Mount Scott granite and on the experimental setting and results can be found in Katz *et al.* (2001) and Katz & Reches (2004).

VISCOELASTIC DAMAGE RHEOLOGY

The main features of the viscoelastic damage rheology are outlined below. Detailed theoretical background and comparisons with rock mechanics experiments may be found in Lyakhovsky *et al.* (1997a,b) and Hamiel *et al.* (2004a). Following these authors our formulation accounts for three general aspects of rock deformation:

(i) A mechanical aspect—the effective elastic moduli of the cracked solid are assumed to depend on a simple scalar, termed material damage.

(ii) A kinetic aspect—the damage evolves as a function of the ongoing deformation.

(iii) A dynamical aspect—macroscopic instability occurs at a critical level of damage.

To evaluate the damage effects Lyakhovsky *et al.* (1997b) generalize the elastic strain energy potential of a deforming solid to the form:

$$U = \frac{1}{\rho}\left(\frac{\lambda}{2}I_1^2 + \mu I_2 - \gamma I_1\sqrt{I_2}\right). \tag{2}$$

The elastic energy potential (2) includes two quadratic Hookean terms of the elastic strain tensor ε_{ij} with the Lamé moduli λ and μ and an additional non-linear second-order term with strain coupling modulus γ. $I_1 = \varepsilon_{ii}$ and $I_2 = \varepsilon_{ij}\varepsilon_{ij}$ are two independent invariants of the elastic strain tensor, and ρ is the rock density. Differentiation of the elastic energy (2) leads to constitutive stress–strain relation for the stress tensor, σ_{ij}

$$\sigma_{ij} = \rho\frac{\partial U}{\partial \varepsilon_{ij}} = \left(\lambda - \frac{\gamma}{\xi}\right) I_1\delta_{ij} + 2\left(\mu - \frac{1}{2}\gamma\xi\right)\varepsilon_{ij}, \tag{3}$$

where $\xi = I_1/\sqrt{I_2}$ is a strain invariant ratio ranging from $\xi = -\sqrt{3}$ for isotropic compaction to $\xi = \sqrt{3}$ for isotropic dilation. Eq. (3) reduces to linear Hookean elasticity for an undamaged solid ($\gamma = 0$). The cumulative effect of distributed microcracks and flaws in the elastic material leads to reduction of the effective elastic moduli and non-linear elasticity with asymmetric response to loading under tension and compression conditions. Eq. (3) can be expressed though the dependence of the effective elastic moduli ($\lambda^e = \lambda - \gamma/\xi$; $\mu^e = \mu - \gamma\,\xi/2$) on the strain invariant ratio and their abrupt change with transition from compacting ($\xi < 0$) to dilating ($\xi > 0$) strains. Change in the effective elastic moduli under stress reversal in a four-point beam test (Weinberger *et al.* 1994), rock dilation due to deviatoric stresses (Hamiel *et al.* 2005b) and other rock mechanics experiments (Lyakhovsky *et al.* 1993, 1997b) confirm the applicability of the non-linear stress–strain relations (3) derived from the potential (2).

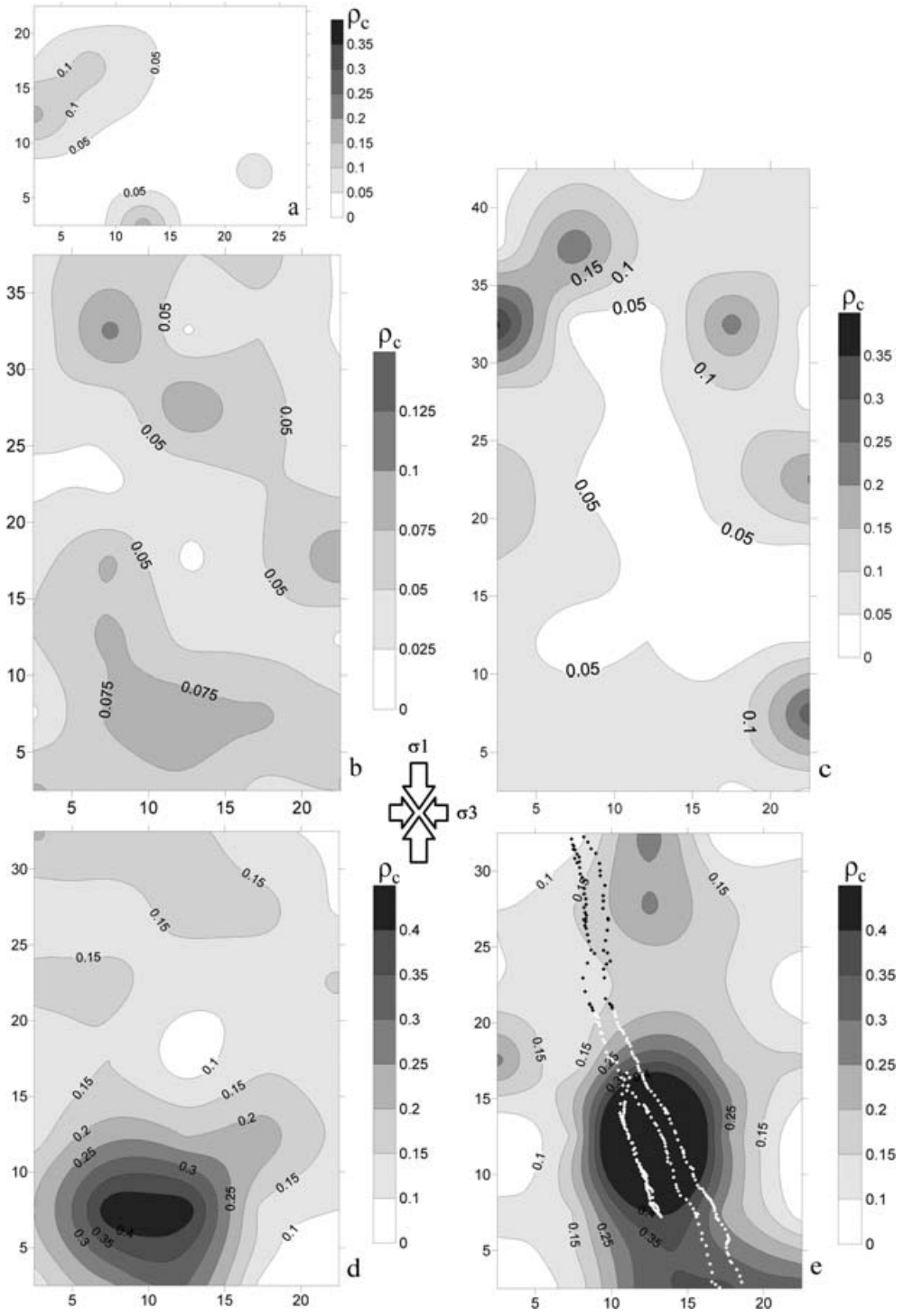

Figure 2. Local values of the microcrack density, ρ_c, calculated from the fracture maps of Katz & Reches (2004) using eq. (1). (a–e) are samples 157, 123, 114, 113 and 110, respectively. Contours indicate the values of ρ_c (note that not all the samples are on the same scale), and diamonds (black and white) in sample 110 (e) are the fault trace (not included in the calculations of microcrack density); black and white colors of diamonds are used for clarity. Maps show the x (σ 3) $-$ z (σ1) plane of the samples except for the not loaded sample 157 (a) which shows x–y plane.

The effect of rock degradation is achieved by changing the elastic moduli functions of a scalar damage variable α, that is, $\lambda(\alpha)$, $\mu(\alpha)$ and $\gamma(\alpha)$. α ranges between 0 and 1, where in undamaged material $\alpha = 0$, and failure occurs at critical α. Using the balance equations of energy and entropy, and accounting for irreversible changes related to viscous deformation and material damage, the equation of damage evolution has the form (Lyakhovsky *et al.* 1997a)

$$\frac{d\alpha}{dt} = -C\frac{\partial U}{\partial \alpha}, \tag{4}$$

where the positive constant or function of state variables C provides the non-negative local entropy production related to damage

Table 1. Experimental conditions and calculated microcrack density of the analysed samples.

Test	Test type	Hold stress[a] (MPa/fraction)	Hold time[b] (Minutes)	Microcrack density ρ_c (eq. 1)
157	Not loaded	0/0	0	0.037 ± 0.034
123	Load-Hold	334/0.57	180	0.049 ± 0.005
114	Load-Hold	518/0.88	180	0.068 ± 0.015
113	Load-Hold	563/0.96	180	0.145 ± 0.048
110	Spontaneous failure	564/0.96	0.03	0.152 ± 0.071

[a]Maximum differential stress/fraction of the ultimate strength ($U_S = 586$ MPa) at the start of holding.
[b]Time elapsed from start of stroke holding to unload or failure.

evolution. Eq. (4) can describe not only damage increase or material degradation, but also the process of material recovery associated with healing of microcracks. The latter is favoured by high confining pressure, low shear stress and high temperature. In the context of the laboratory experiments discussed in this study this process is not relevant.

To account for possible stable weakening Hamiel *et al.* (2004a) suggested power-law relations between the damage variable and elastic moduli:

$$\lambda = \text{const.}; \quad \mu = \mu_0 - \mu_1 \alpha; \quad \gamma = \gamma_1 \frac{\alpha^{1+\beta}}{1+\beta}, \tag{5}$$

where $\mu_0, \mu_1, \gamma_1, \xi_0$ and β are constants for each material. Substituting (2) into (4) using (5), the damage evolution can be rewritten as

$$\frac{d\alpha}{dt} = C_d I_2 \left(\alpha^\beta \xi - \xi_0\right), \tag{6}$$

where $C_d > 0$ describes the rate of damage evolution for a given deformation, and ξ_0 is material property. The proposed power-law relation (5) between the damage variable and elastic modulus, γ, leads to a non-linear coupling between the rate of damage evolution and the damage variable itself. Eq. (5) gives rise to three types of damage evolution: (I) healing or damage decrease for $\xi < \xi_{\text{tran}}(\alpha) = \xi_0/\alpha^\beta$; (II) stable damage growth or steady-state solution for damage existing for $\xi_{\text{tran}} \le \xi < \xi_0$; and (III) unstable weakening for $\xi \ge \xi_0$. In the stable regime (II) damage grows asymptotically only to a certain level but not to a level of complete failure ($\alpha < 1$). The transition between different regimes of damage evolution in the strain field for triaxial loading test is schematically shown in Fig. 3. The onset of damage in the model with the power-law relations between the damage variable and elastic moduli (5) depends not only on the material property, ξ_0, but also on the pre-existing level of damage. Using this model, Hamiel *et al.* (2004a) showed that in cyclic loading the yield stress, the stress at the onset of damage, increases from cycle to cycle as it was reported by several laboratory observations and is know as Kaiser effect. The material strength or differential stress at the transition from stable to unstable fracturing for a given confining pressure decreases with damage accumulation. The more damaged the sample is, the lower will be the stress at which failure occurs. This change in the rock strength will be discussed later in this paper.

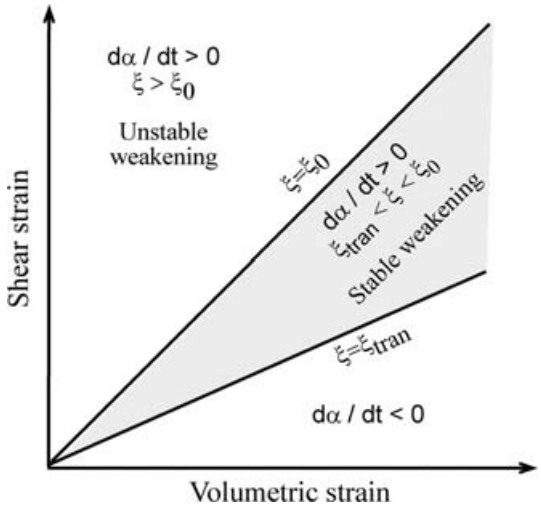

Figure 3. Schematic diagram of the states of strain associated with unstable and stable material weakening, and healing in our model. Unstable weakening occurs when $\xi \ge \xi_0$; stable weakening occurs when $\xi_{\text{tran}} \le \xi < \xi_0$; and healing occurs when $\xi < \xi_{\text{tran}}$.

Comparison between theoretical predictions and the observed deformation and acoustic emissions from laboratory experiments in granites and sandstones led Hamiel *et al.* (2004a) to incorporate gradual accumulation of a damage-related non-reversible deformation. This irreversible (inelastic) strain, ε_{ij}^v, starts to accumulate with the onset of acoustic emission and the rate of its accumulation is suggested to be proportional to the rate of damage increase:

$$\frac{d\varepsilon_{ij}^v}{dt} = \begin{cases} C_v \frac{d\alpha}{dt} \sigma_{ij}^d & \frac{d\alpha}{dt} > 0 \\ 0 & \frac{d\alpha}{dt} \le 0 \end{cases}, \tag{7}$$

where C_v is suggested to be a material constant and σ_{ij}^d is the deviatoric stress tensor. The effective fluidity or inverse of viscosity ($C_v d\alpha/dt$) relates the deviatoric stress to the rate of irreversible strain accumulation. Following Maxwell viscoelastic rheology model the total strain tensor, $\varepsilon_{ij}^{\text{tot}}$, is assumed to be a sum of the elastic strain tensor and the irreversible viscous component of deformation, that is, $\varepsilon_{ij}^{\text{tot}} = \varepsilon_{ij} + \varepsilon_{ij}^v$. This model assumption means that the total irreversible strain accumulated during the loading should be proportional to the overall damage increase in the tested rock sample.

ANALYSIS OF LABORATORY OBSERVATIONS

The continuous monitoring of load, axial and transversal strain components during experiments that involve load-hold tests enables one to constrain damage rheology coefficients and compare the measured microcrack density with calculated damage. In this section, we first constrain our model coefficients using the experiments. Then, we compare the measured and predicted stress–strain curves at different regimes of damage evolution. We discuss the relation between the measured microcrack density and the damage variable, and finally, we compare the measured and predicted rock strength.

The measured stress–strain curves for the Mount Scott granite samples clearly show two different stages of deformation. During the first stage, the stress–strain relations for both axial and

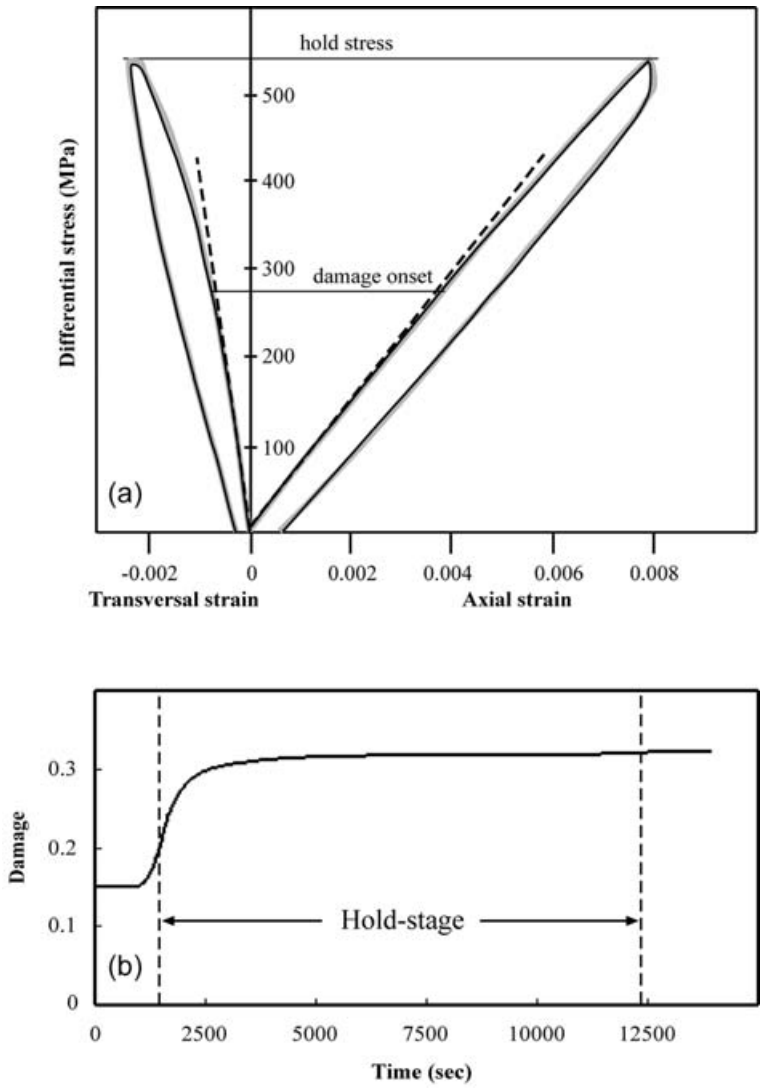

Figure 4. (a) Measured stress–strain curves, axial and transversal, for sample 109 (grey line) compared to the model prediction (black line). Dashed line represents the solution assuming linear elasticity. The values of the hold stress and onset of damage are shown by thin black lines. (b) Simulated evolution of damage (α) during the experiment. See Table 2 for model coefficients.

transversal components exhibit almost linear relations, until approximately 250 MPa differential stress, while during the next stage these relations significantly deviate from the straight line (dash line in Figs 4a, 5a and 6a). We use the linear part of the stress–strain curves to evaluate the initial elastic moduli ($\lambda = 2 \times 10^4$ MPa, $\mu_0 = 3 \times 10^4$ MPa) for all the samples. The point where the stress–strain curve deviates from linear relation allows one to estimate the yield stress and calculate the transitional strain invariant ratio (ξ_{tran}) at the onset of damage. For given values of initial damage (α) and power β (eq. 6), the critical strain invariant ratio is calculated directly ($\xi_0 = \xi_{\text{tran}}\, \alpha^{\beta}$). Estimation of the model coefficients controlling the rate of damage accumulation, β and C_d, is required for the analysis of the entire stress–strain curves from the onset of damage to unloading or failure. To reduce an uncertainty in the evaluation of these model coefficients, we start the analysis using the elastic damage rheology model that ignores gradual accumulation of irreversible strain (7). After fitting the loading path and hold period, we use the model coefficients obtained from the elastic damage rheology model to analyse once again the entire experimental stress–strains accounting for the gradual irreversible strain accumulation. This approach gives rise to improved fitting of the unloading path with a minor change of the loading path. Therefore, the value C_v is estimated only for samples that where completely unloaded after the hold stress. In all calculations we chose the same relatively low level of the initial damage $\alpha = 0.15$. Hamiel *et al.* (2004a) estimated β value (eq. 6) for Westerly granite and Berea sandstone to be 0.15 and 0.5, respectively. In this study we adopt $\beta = 0.4$, that together with other coefficients of the viscoelastic damage rheology model presented in Table 2 provides a good fit to the measured stress–strain curves. Variability of the model coefficients most likely reflects the initial heterogeneity of the granite expressed by the different strengths reported by Katz & Reches (2004). Figs 4(a), 5(a) and 6(a) show the measured and calculated axial and transversal stress–strain curves for samples 109, 115 and 103, respectively. We present the samples 109 (Fig. 4) and 115 (Fig. 5) for load-hold tests experiments because both were loaded to about the same hold stress (546 and 534 MPa, respectively), but different hold time. The sample 109 was held 180 min at a constant stress, while sample 115 was held 360 min. Therefore, they accumulate different damage and irreversible deformation during the experiment. The dotted

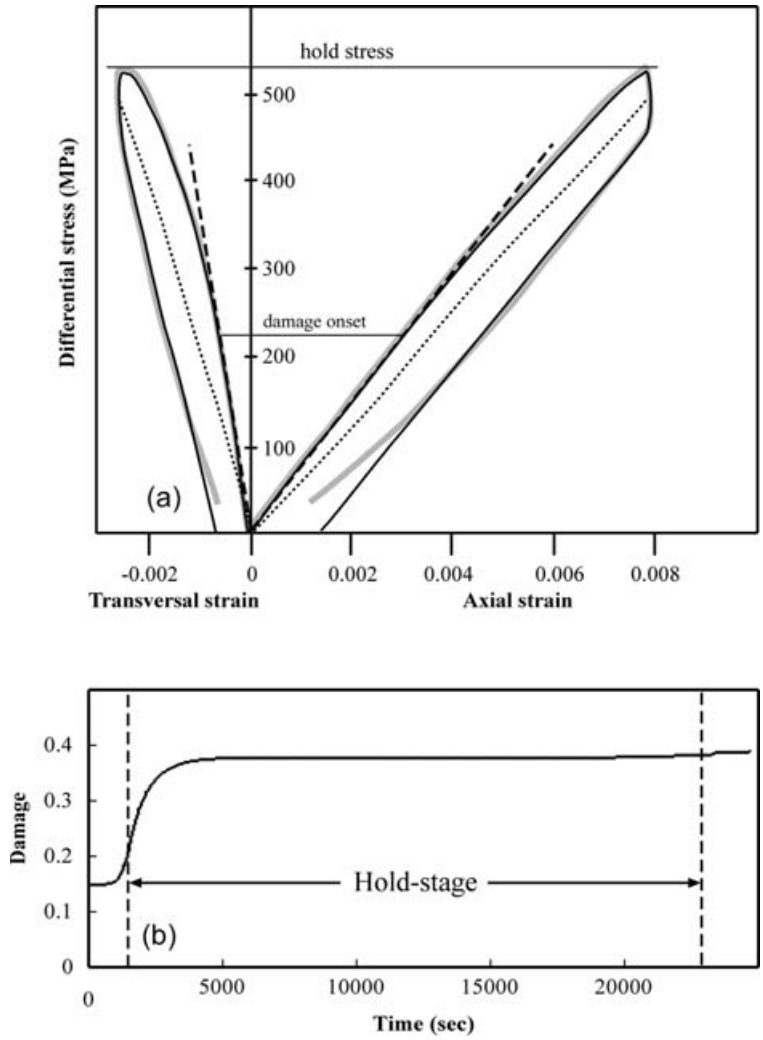

Figure 5. (a) Measured stress–strain curves, axial and transversal, for sample 115 (grey line) compared to the model prediction (black line). Dashed line represents the solution for linear elasticity, and dotted line represents the solution for the elastic damage model, without accumulation of irreversible strain ($C_v = 0$). The values of the hold stress and onset of damage are shown by thin black lines. (b) Simulated evolution of damage (α) during the experiment. See Table 2 for model coefficients.

line in Fig. 5a represents the solution obtained by the elastic damage rheology ignoring gradual accumulation of irreversible strain ($C_v = 0$). The difference between the dotted lines, on one hand, and the solid grey and black lines, on the other hand, for the unloading path in Fig. 5(a) demonstrates an improvement in the predictive power of our model using viscoelastic damage rheology ($C_v > 0$). Note that estimated value of $C_v = 2.0 \times 10^{-5}$ MPa^{-1} for the sample 115 is slightly larger than $C_v = 1.5 \times 10^{-5}$ MPa^{-1} estimated for the sample 109 according to the amount of accumulated irreversible strain. The estimated C_v values for other samples vary between 1×10^{-5} to 2×10^{-5} MPa^{-1} (Table 2). Fig. 6 presents an example for sample 103 that was loaded to complete failure and fitted using elastic damage rheology.

The history of damage accumulation during sample loading is demonstrated in Figs 4b, 5b and 6b, respectively. At the initial stage of loading damage remains constant and equal to the same initial level $\alpha = 0.15$ for all the samples until the onset of damage. At the loading conditions corresponding to $\xi = \xi_{tran}$ (Fig. 3) damage starts to accumulate with increasing rate of damage accumulation. During the loading of the samples 109 and 115 the strain invariant ratio exceeds its transient value ($\xi > \xi_{tran}(\alpha) = \xi_0/\alpha^{\beta}$), but remains below the critical value ($\xi < \xi_0$). In this case a new steady state solution for damage ($\alpha = (\xi_0/\xi)^{1/\beta}$) exists and rate of damage accumulation decreases toward this solution for samples 109 and 115 (Figs 4b and 5b). Most of the damage is accumulated during the first ~5000 s of loading and then remains about constant till the end of the test. Unlike the stable fracturing of the samples 109 and 115, during the loading of the sample 103 (loaded-to-failure) ξ exceeds ξ_0 and, therefore, damage growth is unstable (Fig. 3). The rate of damage accumulation constantly increases from onset to the total failure of the sample 103 (Fig. 6b).

The model results for all the samples (Figs 4–6) confirm that the viscoelastic damage rheology with power-law relation between damage variable and modulus γ (5) adequately represents the laboratory data, and reproduces the different fracturing regimes revealed by experiments with Mount Scott granite.

The essential part of the modelling of sample loading with coefficients obtained from fitting the stress–strain data for these samples (Table 2) is calculation of the damage evolution and estimation of the final damage accumulated during the whole cycle including loading, hold stress and unloading stages. Fig. 7 shows comparisons between the measured and calculated stress–strain (axial and

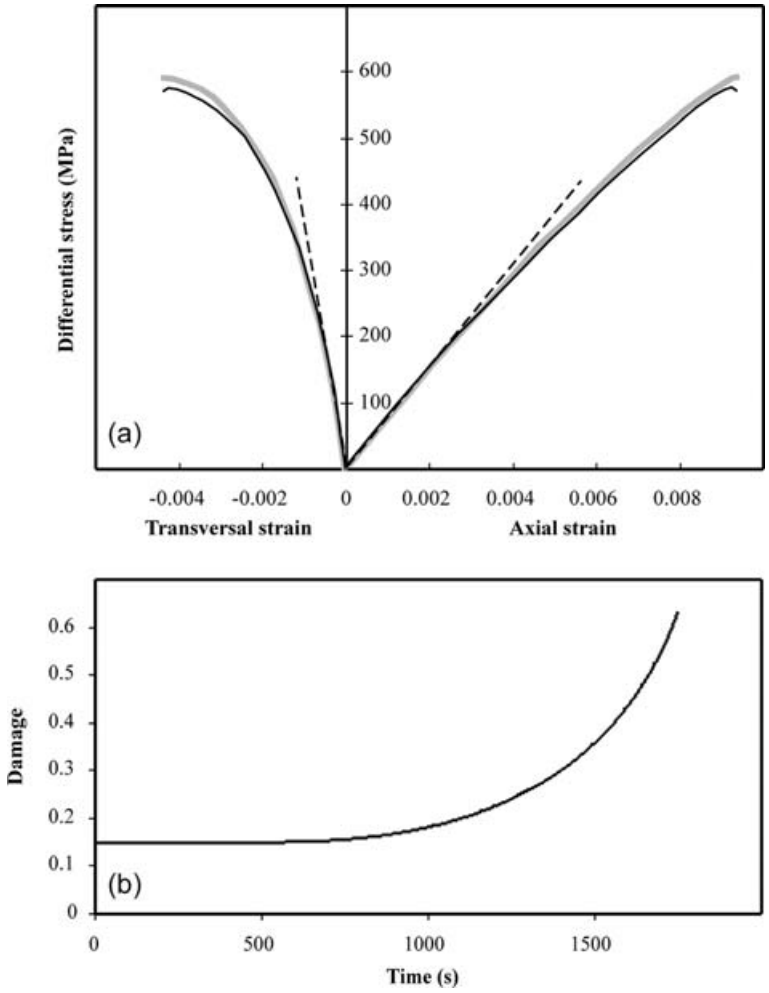

Figure 6. (a) Measured stress–strain curves, axial and transversal, for sample 103 (grey line) compared to the model prediction (black line). Dashed line represents the solution for linear elasticity. (b) Simulated evolution of damage (α) during the experiment. Note the different damage evolution here compared to the load hold tests 109 (Fig. 4) and 115 (Fig. 5).

Table 2. Experimental conditions and model coefficients obtained from fitting the measured stress–strain data (for all tests $\lambda = 2 \times 10^4$ MPa, $\mu_0 = 3 \times 10^4$ MPa).

Test	Hold time (min)	Hold stress (MPa)	Failure stress (MPa)	ξ_0	C_d (1/s)	C_v (1 MPa^{-1})	$R = C_v\,\mu_0$
102	95	601		−0.45	10	1.0×10^{-5}	0.3
103			595	−0.6	40	—	
109	180	546		−0.5	20	1.5×10^{-5}	0.45
110	0.03	564	561	−0.6	50	—	
113	180	563		−0.5	20	1.0×10^{-5}	0.3
114	180	518		−0.45	20	1.5×10^{-5}	0.45
115	360	534		−0.5	20	2.0×10^{-5}	0.6
117	180	318		−0.5	20	—	
123	180	334		−0.46	20	—	

transversal) curves for the samples that were loaded and then analysed for microcrack density (samples 110, 113, 114, 123). As shown in the figure there is a quantitative agreement between the damage model and the experimental observations. Fig. 8 shows the connection between the calculated damage and measured microcrack density, ρ_c, for the five analysed samples (including the non-loaded sample 157; for more details see Table 1). The value of microcrack density measured for the non-loaded sample 157 corresponds to the initial value of $\alpha = 0.15$ adopted in our simulations for the starting material. As shown in Fig. 8 linear regression provides a reasonable connection between the microcrack density and the damage variable:

$$\alpha = 4.5(\pm 0.5) \cdot \rho_c. \tag{8}$$

This relation means that the shear elastic modulus μ decreases linearly with the increase of microcracks density. However, increasing the elastic modulus γ, from zero for a linear-elastic damage-free

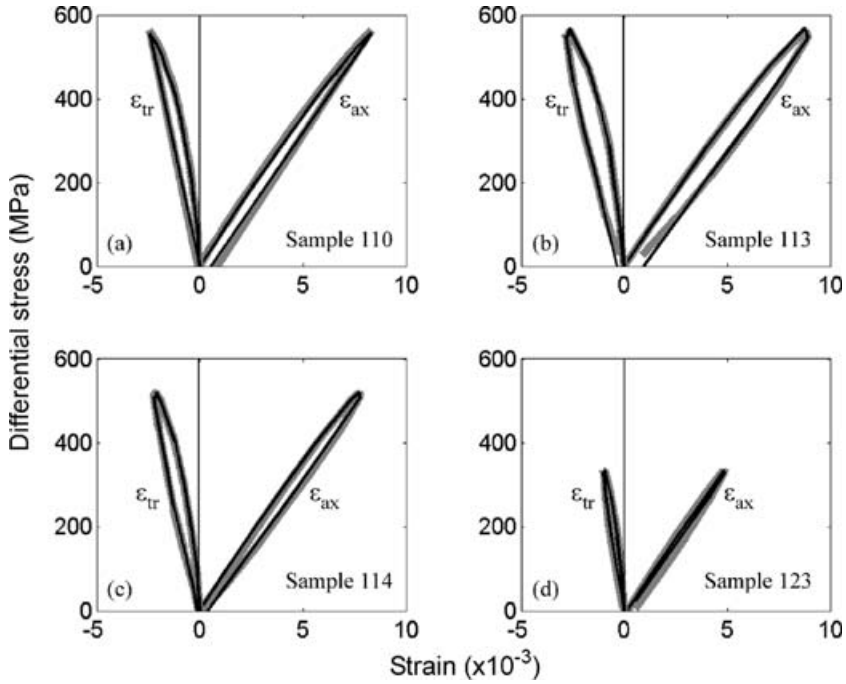

Figure 7. Measured stress–strain curves (grey line), axial and transversal, for samples that were loaded and then analysed for crack density [samples: 110 (a), 113 (b), 114 (c), 123 (d)] compared with the calculated curve (black line). For model coefficients see Table 2.

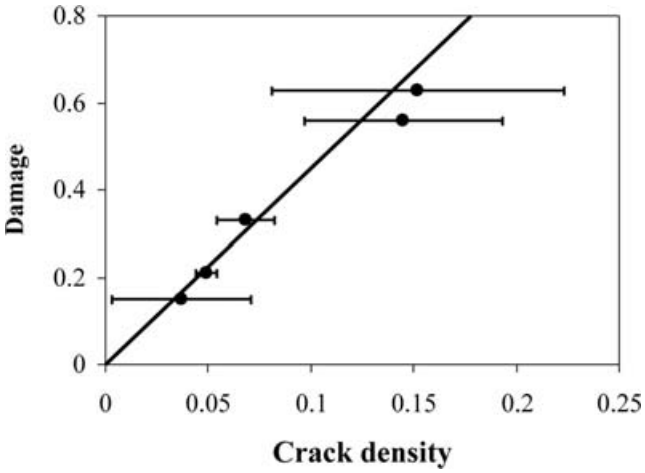

Figure 8. The measured crack density, ρ_c, versus the calculated damage variable, α. The inferred linear relation $\alpha = 4.5\rho_c$ is shown by black line.

material to its maximum value at the critical damage, amplifies the material non-linearity with damage accumulation.

The laboratory experiments preformed by Katz *et al.* (2001) show an increase in the strength of Mount Scott granite samples with confining pressure (Fig. 9a). The maximum differential stresses for all the hold-tests are also shown in Fig. 9(a). Lyakhovsky *et al.* (1997a, 2005) demonstrated that the damage rheology provides a good fit to observed sample strength for relatively high confining pressures (above 100 MPa), but significantly overestimates the strength of Westerly granite at low confining pressures. Similar to the results of Lyakhovsky *et al.* (1997a, 2005), the model with constant value of the damage rate parameter $C_d \cong 20$ s^{-1} (Table 2) provides a good fit to observed data for relatively high confining pressures (above 40 MPa) for the strength of Mount Scott granite samples, but significantly overestimates the strength values at low confining pressures (not shown here). Following Lyakhovsky *et al.* (2005) we use a pressure-dependent C_d that decays exponentially with characteristic pressure scale of 14 MPa (Fig. 9b). Two calculated yield curves, that is, strength versus confining pressure, are presented in Fig. 8(a), one with $\xi_0 = -0.6$ and the other with $\xi_0 = -0.5$. The value of the critical strain invariant ratio for most of the samples (Table 2) falls into this interval corresponding to the variation of the strength value reflecting the inherent heterogeneity of the granite. The change of ξ_0 from -0.6 to -0.5 leads to onset of damage at higher strain (or stress) and, therefore, higher failure stress. Thus, the yield curve for $\xi_0 = -0.5$ is at higher stresses than the same for $\xi_0 = -0.6$. As shown in Fig. 8(a) all the measured data, except for zero confining pressure, fall between these two curves. The low value of the measured rock strength at zero confining pressure indicates that the damage rate in the vicinity of zero confining pressure is probably even higher than those constrained here. It should be noted that the inferred coefficient C_d is approximately constant for pressures above 30 MPa, indicating that constant value may be adopted for simulations of fracture processes in the seismogenic zone.

DISCUSSION

Experimental verification of viscoelastic damage rheology

We tested the viscoelastic damage rheology introduced by Hamiel *et al.* (2004a) against two new sets of laboratory experiments with Mount Scott granite. Thus we extended previous results that were based on experiments with Westerly granite and Berea sandstone samples (Hamiel *et al.* 2004a) and provided additional constraints on the coefficients of damage rheology. An advantage of the new experiments with Mount Scott granite is that they have been performed with different loading paths and explicitly demonstrated the existence of stable and unstable fracturing regimes. Some of the samples were loaded to failure under different confining pressures,

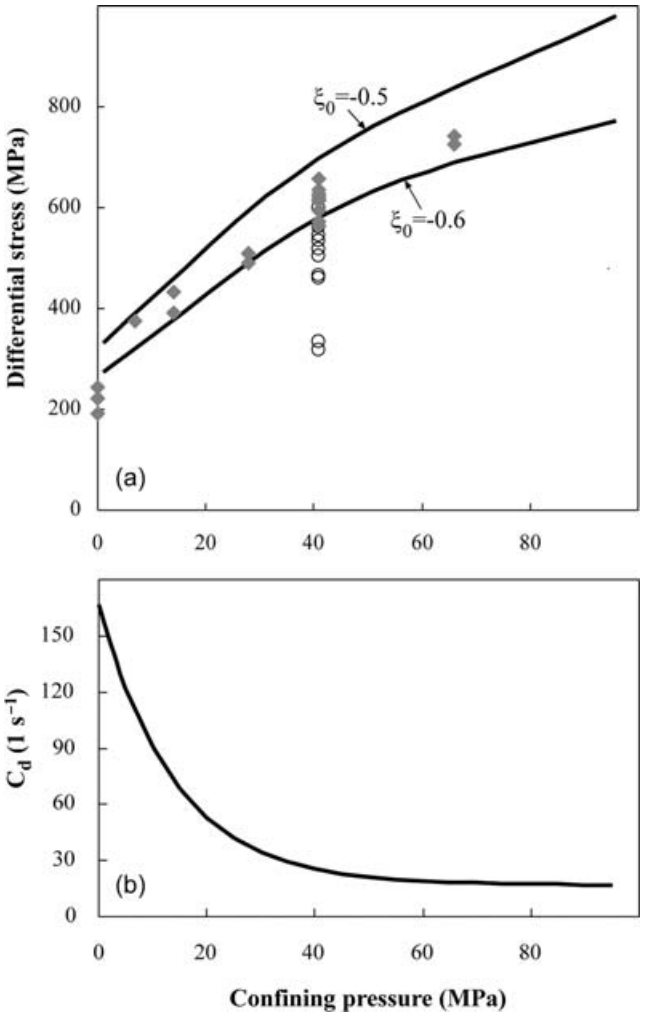

Figure 9. (a) The measured failure stress versus confining pressure (grey diamonds) compared with calculated failure curves for $\xi_0 = -0.5$ and $\xi_0 = -0.6$ ($C_v = 1.5 \times 10^{-5}$ MPa^{-1}). The stress at which the load-hold experiments were held (without failure of the sample) is shown by empty black circles. (b) The damage rate coefficient, C_d, versus confining pressure used for calculating the curves for the Mount Scott granite shown in (a).

while others were held at constant stress lower than the long-term strength and then gradually unloaded by reducing the axial stress to the confining pressure. This allows a detailed study of the rock behaviour under different conditions including various amounts of irreversible strain accumulated during the cycle. Figs 4–7 and 9 demonstrate that viscoelastic damage rheology provides an adequate quantitative mathematical description of the brittle rock deformation and simulates both the stable and unstable damage evolution under various loading conditions.

The results of simulations with model coefficients presented in Table 2 provide a reasonable fit to the experimental data. However, the presented set of model parameters is not unique. The measured variability of the failure stress could be accounted for by choosing slightly different critical strain invariant ratio ξ_0 or different initial level of damage, or both. The elastic moduli estimated from the initial linear stage of deformation are about the same for all the samples. This observation leads us to assume that the initial level of damage is the same for different samples. Variability of the estimated critical strain invariant ratio, ξ_0, controlling the transition from stable to unstable fracturing reflects the inherent heterogeneity of the granite samples discussed by Katz & Reches (2004). There exists some trade-off between the adopted assumed level of starting material ($\alpha = 0.15$) and the critical strain invariant ratio, ξ_0. Assuming larger initial damage ($\alpha = 0.2$) requires decreasing ξ_0 from -0.5 to $\xi_0 = -0.55$ for the onset of damage at the same stress. In both cases the entire stress–strain curves could be fitted reasonably well without significant variations in the other model parameters. The available experimental data do not allow a unique constraint on the model parameters without additional sample tests.

The two kinetic coefficients C_d and C_v controlling the rate of damage accumulation and damage-related irreversible strain accumulation are much better constrained with the available data than the other model parameters. C_d dramatically affects the shape of the stress–strain curve between onset of damage and failure, while changes in C_v barely affect the amplitude of failure stress. C_v is mainly constrained using data from the unloading stage. The simulated loading path for the pure elastic ($C_v = 0$) and viscoelastic ($C_v \sim 10^{-5}$ MPa^{-1}) damage models shown in Fig. 5 can be hardly distinguished, but there is a big difference in the simulated unloading part using these models. Therefore, we report the values of coefficient C_v (Table 2) only for samples that were unloaded after holding under constant stress. Set of load-to-failure samples under different confining pressures allows constraining pressure-dependency of the damage rate coefficient $C_d(P)$. The results show that large C_d values should be adopted only under low confining pressures (below 30 MPa) and thus are not relevant for the fracture process in the seismogenic zone at depths greater than 1–2 km.

Damage-related viscosity and seismic coupling

The series of load-hold tests (Katz & Reches 2004) analysed here allow direct estimation of the strain partitioning between elastic and inelastic components based on the laboratory data. Ben-Zion & Lyakhovsky (2006) connected the rate of irreversible strain accumulation with partitioning between seismic and aseismic deformation in the seismogenic zone, or seismic coupling. They use a non-dimensional value $R = \mu_0 \cdot C_v$ and showed that the fraction of elastic strain released during a seismic cycle, that is, the seismic coupling, χ, can be estimated as

$$\chi = \frac{1}{1+R}. \tag{9}$$

The R-value represents the ratio between timescale of damage accumulation and the timescale of the damage-related irreversible strain accumulation under a given loading conditions and is the major factor controlling the aftershock productivity and the rate of aftershock decay. Ben-Zion & Lyakhovsky (2006) also demonstrated that long aftershock sequences fitted well by Omori law are expected in regions with $R < 1$, or large seismic coupling, $\chi > 50$ per cent. This theoretical prediction is supported by previous estimates of R value for Westerly Granite (Hamiel *et al.* 2004a) and estimates for Mount Scott granite presented in this study (Table 2). For all granite samples the R value falls between 0.3 and 0.6 corresponding to seismic coupling $60 < \chi < 80$ per cent. Previous analyses of experimental results with Berea sandstone indicate that the latter accumulates more irreversible strain, that is, $R = 1.4$ corresponding to $\chi =$ 42 per cent (Hamiel *et al.* 2004a). A comparison between different types of rocks, that is, granites and sandstones, enables one to relate the seismic coupling to the lithology. We suggest that granular rocks or rocks with higher porosity have lower seismic coupling. This implies that the portion of elastic strain released during a seismic cycle as brittle deformation depends on the lithology of the region. For

example, fault zones that comprise significant accumulation of gouge or regions that have thick sedimentary cover are expected to release more energy by aseismic slip. The dependence of χ on the lithology might provide an explanation for the shallow slip deficit reported by Fialko *et al.* (2005) for some large earthquakes. However, to date there exist only few observational constraints on the depth distribution of fault slip averaged over multiple earthquake cycles, and in different host rocks. The lack of such constraints impedes robust conclusions about the effect of the fault zone lithology on the degree of seismic coupling. Further work is required to test our model predictions. It should also be noted that all the laboratory experiments reported in this study were performed at room temperature and relatively low confining pressures. We are aware that the rate of irreversible strain accumulation (R value) may be significantly different under high temperatures, presumably leading to reduced seismic coupling.

Measured microcrack density and calculated damage variable

The results of simulations based on the damage rheology approach are applicable to volumes with a sufficiently large number of cracks that allow quantitative description through properties of the crack distribution rather than those of the individual cracks. The damage variable, α, represents the change of the effective elastic moduli and is connected to the microcrack density. Linear and non-linear expressions for the effective elastic moduli of damaged rocks as a function of microcrack density have been suggested (see review by Kachanov 1992), but their experimental verifications have been rather limited. Katz & Reches (2004) presented the first experimental support for the connection between experimentally measured microcrack density and reduction in the Young modulus predicted by the model of the elastic isotropic solid with randomly distributed non-interacting microcracks (e.g. Kachanov 1992). In the present study the damage variable is constrained based on fitting the entire stress–strain records, and found to be a linear function of the microcrack density ρ_c (Fig. 8). The linear relation between α and ρ_c (8) is in agreement with the theoretical prediction of Kachanov (1992) and with a previous comparison between the calculated rate of damage accumulation and measured acoustic emission (Hamiel *et al.* 2004a). However, in the damage rheology presented in this paper, the linear relation between α and ρ_c does not imply a linear Hookean elasticity or a linear reduction in the elastic moduli. The assumption of open stationary cracks implemented by the self-consistent (O'Connell & Budiansky 1974; Budiansky & O'Connell 1976) and similar schemes (e.g. Bruner 1976; Henyey & Pomphrey 1982; Kachanov 1992) forces the macroscopic elastic stress–strain relations to be linear. Following Lyakhovsky *et al.* (1997b), in addition to the quadratic terms of the Hookean elastic solid, our model includes a non-analytical, second-order term $I_1\sqrt{I_2}$ in the energy expression (2). Thus, our model accounts for microcracks dilation and closure due to changes in the crack-normal stress and leads to non-linear stress–strain relations even for small strains. The relation (8) means that only the shear elastic modulus μ decreases linearly with an increase of microcracks density ρ_c. The third elastic modulus, γ, increases from zero for a linear-elastic damage-free material to its maximum value at the critical damage, according to the power-law relation (5). Hence, the material non-linearity is amplified with the damage accumulation.

The damage variable, α, and the microcrack density, ρ_c, characterize a properly chosen volume of rock with a large number of internal flaws (microcracks in a laboratory specimen or small faults in the Earth's crust) and are not related to any intrinsic length scale. Therefore, we suggest that the linear relation between α and ρ_c (8) should be scale independent and hold on a scale of the thickness of the brittle crust.

ACKNOWLEDGMENTS

We thank Cindy Ebinger and two anonymous reviewers for their constructive reviews. The authors gratefully acknowledge support from the Green Foundation (YH), Israel Ministry of Infrastructures (grant 24-17-022), the US-Israel Binational Science Foundation (grant 2004046), the National Science Foundation (grant EAR-0450035 made to YF), and the Southern California Earthquake Center (SCEC).

REFERENCES

Auth, C., Bercovici, D. & Christensen, U.R., 2003. Two-dimensional convection with self-lubricating, simple-damage rheology, *Geophys. J. Int.,* **154,** 783–800.

Ben-Avraham, Z. & Lyakhovsky, V., 1992. Faulting process along the northern Dead Sea transform and Levant margin, *Geology,* **20,** 1139–1142.

Ben-Avraham, Z., Lyakhovsky, V. & Grasso, M., 1995. Simulation of the collisional zone segmentation in the Central Mediterranean, *Tectonophysics,* **243,** 57–68.

Ben-Zion, Y. & Lyakhovsky, V., 2002. Accelerating seismic release and related aspects of seismicity patterns on earthquake faults, *Pure appl. Geophys.,* **159,** 2385–2412.

Ben-Zion, Y. & Lyakhovsky, V., 2006. Analysis of aftershocks in a lithospheric model with seismogenic zone governed by damage rheology, *Geophys. J. Int.,* **165,** 197–210.

Ben-Zion, Y., Dahmen, K., Lyakhovsky, V., Ertas, D. & Agnon, A., 1999. Self-driven mode switching of earthquake activity on a fault system, *Earth planet. Sci. Lett.,* **172,** 11–21.

Bercovici, D., 2003. The generation of plate tectonics from mantle convection, *Earth planet. Sci. Lett.,* **205,** 107–121.

Bercovici, D. & Ricard, Y., 2005. Tectonic plate generation and two-phase damage: void growth versus grainsize reduction, *J. geophys. Res.,* **110,** B03401, doi:10.1029/2004JB003181.

Bruner, W.M., 1976. Comments on 'Seismic velocity in dry and saturated cracked solids' by O'Connell & Budiansky, *J. geophys. Res.,* **81,** 2573–2576.

Budiansky, B. & O'Connell, R.J., 1976. Elastic moduli of a cracked solid. *Int. J. Solids Struct.,* **12,** 81–97.

Fialko Y., 2004. Probing the mechanical properties of seismically active crust with space geodesy: study of the coseismic deformation due to the 1992 Mw7.3 Landers (southern California) earthquake, *J. geophys. Res.,* **109,** B03307, doi:10.1029/ 2003JB002756.

Fialko, Y., Sandwell, D., Agnew, D., Simons, M., Shearer, P. & Minster, B., 2002. Deformation on nearby faults induced by the 1999 Hector Mine earthquake, *Science,* **297,** 1858–1862.

Fialko, Y., Sandwell, D., Simons, M. & Rosen, P., 2005. Three-dimensional deformation caused by the Bam, Iran, earthquake and the origin of shallow slip deficit, *Nature,* **435,** 295–299.

Hadley, K., 1976. Comparison of calculated and observed crack densities and seismic velocities in Westerly granite, *J. geophys. Res.,* **81,** 3484–3494.

Hamiel, Y., Liu, Y., Lyakhovsky, V., Ben-Zion, Y. & Lockner, D., 2004a. A visco-elastic damage model with applications to stable and unstable fracturing, *J. Geophys. Int.,* **159,** 1155–1165.

Hamiel, Y., Lyakhovsky, V. & Agnon, A., 2004b. Coupled evolution of damage and porosity in poroelastic media: theory and applications to deformation of porous rocks, *Geophys. J. Int.,* **156,** 701–713.

Hamiel, Y., Lyakhovsky, V. & Agnon, A., 2005a. Poroelastic damage rheology: dilation, compaction, and failure of rocks, *Geochem. Geophys. Geosyst.,* **6,** doi:10.1029/2004GC000813.

Hamiel, Y., Lyakhovsky, V. & Agnon, A., 2005b. Rock dilation, Nonlinear deformation, and pore pressure change under shear, *Earth planet. Sci. Lett.,* **237,** 577–589.

Hansen, N.R. & Schreyer, H.L., 1994. A thermodynamically consistent framework for theories of elastoplasticity coupled with damage, *Int. J. Solids Structures,* **31,** 359–389.

Henyey, F.S. & Pomphrey, N., 1982. Self-consistent moduli of a cracked solid, *Geophys. Res. Lett.,* **9,** 903–906.

Homand, F., Hoxha, D., Belem, T., Pons, M.-N. & Hoteit N., 2000. Geometric analysis of damaged microcracking in granites, *Mech. Mat.,* **32,** 361–376.

Janssen, C., Wagner, F.C., Zang, A. & Dresen, G., 2001. Fracture process zone in granite: a microstructural analysis, *Int. J. Earth Sci.,* **90,** 46–59.

Ju, J.W., 1990. Isotropic and anisotropic damage variables in continuum damage mechanics, *J. Eng. Mech.,* **116,** 2764–2770.

Kachanov, M., 1992. Effective elastic properties of cracked solids; critical review of some basic concepts, *Appl. Mech. Rev.,* **45,** 304–335, 1992.

Kachanov, M., 1994. On the concept of damage in creep and in the brittle-elastic range, *Int. J. Damage Mech.,* **3,** 329–337.

Katz, O. & Reches, Z., 2004. Microfracturing, damage, and failure of brittle granites, *J. geophys. Res.,* **109,** B01206, doi:10.1029/2002JB001961.

Katz, O., Gilbert, M.C., Reches, Z. & Roegiers, J.C., 2001. Mechanical properties of Mount Scott granite, Wichita Mountains, Oklahoma, *Oklahoma Geology Notes,* **61,** 28–34.

Krajcinovic, D., 1996. *Damage Mechanics*, pp. 761, Elsevier, Amsterdam, The Netherlands.

Kranz, L.K., 1979. Crack growth and development during creep in Westerly granite, *Int. J. Rock. Mech. Min Sci,* **16,** 23–36.

Kranz, R.L., Harris, W.J. & Carter, N.L., 1982. Static fatigue of granite at 200°C, *J. geophys. Res.,* **9,** 1–4.

Lawn, B., 1993. *Fracture of Brittle Solids*,second edition, pp. 378, Cambridge University Press, Cambridge, UK.

Lockner, D.A. & Byerlee, J.D., 1980. Development of fracture planes during creep in granite, in *2nd conference on acoustic emission/microseismic activity in geological structures and materials*, pp. 11–25, eds Hardy, H.R. & Leighton, F.W., Trans-Tech. Publications, Clausthal-Zellerfeld, Germany.

Lockner, D.A., Byerlee, J.D., Kuksenko, V., Ponomarev, A. & Sidorin, A., 1991. Quasi-static fault growth and shear fracture energy in granite, *Nature,* **350,** 39–42.

Lockner, D.A., Byerlee, J.D., Kuksenko, V., Ponomarev, A. & Sidorin, A., 1992. Observations of quasi-static fault growth from acoustic emissions. in *Fault mechanics and transport properties of rocks, International Geophysics Series*, **Vol. 51,** pp. 3–31, eds Evans, B. & Wong, T.-f., Academic Press, San Diego, California.

Lyakhovsky, V. & Myasnikov, V.P., 1985. On the behavior of visco-elastic cracked solid, *Phys. Solid Earth,* **4,** 28–35.

Lyakhovsky, V., Podladchikov, Y. & Poliakov, A., 1993. Rheological model of a fractured solid, *Tectonophysics,* **226,** 187–198.

Lyakhovsky, V., Ben-Avraham, Z. & Achmon, M., 1994. The origin of the Dead Sea rift, *Tectonophysics,* **240,** 29–43.

Lyakhovsky, V., Ben-Zion, Y. & Agnon, A., 1997a. Distributed damage, faulting, and friction, *J. geophys. Res.,* **102,** 27 635–27 649.

Lyakhovsky, V., Reches, Z., Weinberger., R. & Scott, T.E., 1997b. Nonlinear elastic behavior of damaged rocks, *Geophys. J. Int.,* **130,** 157–166.

Lyakhovsky, V., Ben-Zion, Y. & Agnon, A., 2001. Earthquake Cycle, Fault Zones, and Seismicity Patterns in a Rheologically Layered Lithosphere, *J. geophys. Res.,* **106,** 4103–4120.

Lyakhovsky, V., Ben-Zion, Y. & Agnon, A., 2005. A viscoelastic damage rheology and rate- and state-dependent friction, *Geophys. J. Int.,* **161,** 179–190.

Martin, C.D. & Chandler, N.A., 1994. The progressive fracture of Lac du Bonnet granite, *Int. J. Rock Mech. Min. Sci &Geomech. Abstr.,* **31,** 643–659.

Moore, D.E. & Lockner, D.A., 1995. The role of microcracking in shear-fracture propagation in granite, *J. Struct. Geol.,* **17,** 95–114.

Myasnikov, V.P., Lyakhovsky, V.A. & Podladchikov, Y.Y., 1990. Non-local model of strain-dependent visco-elastic media, *Doklady Acad. Sci. USSR,* **312,** 302–305.

Nanjo, K., Turcotte, D.L. & Shcherbakov, R., 2005. A model of damage mechanics for the deformation of the continental crust, *J. geophys. Res.,* **110,** B07403, doi:10.1029/2004JB003438.

Newman, W.I. & Phoenix, S.L., 2001. Time-dependent fiber bundles with local load sharing, *Physical Rev. E.,* **63,** Art. No. 021507.

Nishihara, M., 1957. Stress-strain relation of rocks, *Doshisha Eng. Rev.,* **8,** 32–54.

O'Connell, R.J. & Budiansky, B., 1974. Seismic wave velocities in dry and saturated cracked solid, *J. geophys. Res.,* **79,** 5412–5426.

Oda, M., Katsube, T. & Takemura T., 2002. Microcrack evolution and brittle failue of Inada granite in triaxial compression tests at 140 MPa, *J. geophys. Res.,* **107,** 2233, doi:2210.1029/2001JB000272.

Papa, E., 1993. A damage model for concrete subjected to fatigue loading, *Eur. J. Mech., A/Solids,* **12,** 429–440.

Pestman, B.J. & Munster, J.G., 1996. An acoustic emission study of damage development and stress—memory effects in sandstone, *Int. J. Rock Mech. Min. Sci. &Geomech. Abstr.,* **33,** 585–593.

Rabotnov, Y.N., 1988. *Mechanics of Deformable Solids*, pp. 712, Science, Moscow, Russia.

Reches, Z. & Lockner, D.A., 1994. Nucleation and growth of faults in brittle rocks, *J. geophys. Res.,* **99,** 18159–18173.

Regenauer-Lieb, K. & Yuen, D.A., 2003. Modeling shear zones in geological and planetary sciences: solid-and fluid-thermal–mechanical approaches, *Earth Sci. Rev.,* **63,** 295–349.

Rubinstein, J.L. & Beroza, G.C., 2004. Nonlinear strong ground motion in the ML 5.4 Chittenden earthquake: evidence that preexisting damage increases susceptibility to further damage, *Geophys. Res. Lett.,* **31,** L23614, doi:10.1029/2004GL021357.

Rundle, J.B., Turcotte, D.L., Shcherbakov, R., Klein, W. & Sammis. C., 2003. Statistical physics approach to understanding the multiscale dynamics of earthquake fault systems, *Rev. Geophys.,* **41,** Art. No. 1019.

Schock, R.N., 1977. The response of rocks to large stresses, in *Impact and Explosion Cratering*, pp. 657–688, eds Roddy, D.L., Pepin, R.O. & Merrill, R.B., Pergamon Press, New York.

Shcherbakov, R. & Turcotte, D.L., 2003. Damage and self-similarity in fracture, *Theoretical Applied Fracture Mechanics,* **39,** 245–258.

Shcherbakov, R. & Turcotte, D.L., 2004. A damage mechanics model for aftershocks, *Pure appl. Geophys.,* **161,** 2379–2391.

Skrzypek, J.J. & Ganczarski, A., 1999. *Modeling of material damage and failure of structures: Theory and applications*, p. 541, Springer, Berlin, Germany.

Tapponnier, P. & Brace, W.F., 1976. Development of stress-induced microcracks in Westerly granite, *Int. J. Rock Mech Min Sci &Geomech Abstr.,* **13,** 103–112.

Turcotte, D.L., Newman, W.I. & Shcherbakov, R., 2003. Micro and macroscopic models of rock fracture, *Geophys. J. Int.,* **152,** 718–728.

Valanis, K.C., 1990. A theory of damage in brittle materials, *Eng. Fract. Mech.,* **36,** 403–416.

Weinberger, R., Reches, Z., Eidelman, A. & Scott, T.S., 1994. Tensile properties of rocks in four-point beam tests under confining pressure, in *Proceedings first North American Rock Mechanics Symposium*, pp. 435–442, eds Nelson, P. & Laubach, S.E., Austin, Texas.

Weinberger, R., Lyakhovsky, V., Baer, G. & Agnon, A., 2000. Damage zone around en-echelon dyke segments in porous sandstone, *J. geophys. Res*., **105,** 3115–3133.

Zang, A., Wagner, C.F. & Dresen, G., 1996. Acoustic emission, microstructure, and damage model of dry and wet sandstone stressed to failure, *J. geophys. Res.,* **101,** 17 507–17 521.

Zoback, M.D. & Byerlee, J.D., 1975. The effect of microcrack dilatancy on the permeability of Western granite, *J. geophys. Res.,* **80,** 752–755.